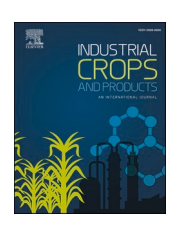
ELSEVIER

Contents lists available at ScienceDirect

Industrial Crops & Products

journal homepage: www.elsevier.com/locate/indcrop





Thermal, chemical and mechanical characterization of *Azadirachta indica* tree gum

Jebaratnam Joy Mathavan^a, Muhammad Hafiz Hassan^{b,*}

- a Department of Engineering Technology, Faculty of Technology, University of Jaffna, Kilinochchi premises, Ariviyal Nagar, Kilinochchi 44000, Sri Lanka
- ^b School of mechanical Engineering, Engineering Campus, Universiti Sains Malaysia, Nibong Tebal, Pulau Pinang 14300, Malaysia

ARTICLE INFO

Keywords: Azadirachta indica tree gum μ X-ray fluorescence test Simultaneous thermal analysis Fourier transform infra-red spectrum Mechanical properties

ABSTRACT

This study focuses on the comprehensive thermal, chemical, and mechanical characterization of neem gum, a natural, colorless, tasteless polysaccharide obtained from Azadirachta indica tree's trunk. The collection process of gum involves manual extraction from crude neem tree exudates, followed by thorough cleaning and homogenization with water. A portion of the resulting gum is then filtered, allowed to thicken, and naturally dried for subsequent mechanical testing. Various analytical techniques, such as thermogravimetric analysis (TGA), and differential scanning calorimetry (DSC) to determine the thermal properties, Fourier transform infrared spectrometry (FTIR) to find the functional groups, scanning electron microscopy (SEM), and micro-X-ray fluorescence analysis (µ-XRF) to decide the elemental composition, microhardness, tensile, flexural, and compression tests to determine the mechanical properties, are employed in this study. The thermal and mechanical properties of neem gum have been relatively unexplored, and this highlights the novelty and importance of this research. The results are analyzed and compared with other natural tree gums. The pH of 5.07 shows that the gum is slightly acidic in nature, and the peaks obtained from thermal analysis demonstrate that it doesn't have a melting point. The microhardness value, tensile strength, flexural strength, and compressive strength of neem gum are 238.64 MPa, 1.0155 MPa, 1.899 MPa, and 1.1023 MPa, respectively. This research provides valuable insights into the diverse characteristics and potential applications of neem gum in various fields. It is being used in the pharmaceutical industry. It can also be used as a cap for cutting tools, such as drill bits, after manufacturing, during transportation to protect their sharp edges from damage.

1. Introduction

Recent decades have seen research on biopolymers as a potential alternative to petroleum-based polymers. There is a strong trend towards replacing synthetic materials with natural gums due to their nontoxicity, low cost, safety, and availability (Mirhosseini and Amid, 2012). The term "gum" is generally used to define hydrophilic or hydrophobic molecules of high molar mass that have colloidal properties (Kurt et al., 2016). Gums are fluids that flow spontaneously from trees due to adaptations to climatic conditions (physiological gummosis) or in response to any injury, whether mechanical, such as cutting, or due to the action of microorganisms. These gums dry out when exposed to air (Amos Nussinovitch, 2009). From a chemical standpoint, gums are polysaccharides, composed of polymers of sugars and oxidized sugar linked together by glycosidic bonds. These polysaccharides can decompose into water, carbon dioxide, and inorganic compounds without leaving toxic

residues (Choudhary et al., 2023). The most fundamental properties of a gum that make it unique among polysaccharides are generally high water solubility and low viscosity (Daoub et al., 2018a). Water-soluble gums, also known as hydrocolloids, have various applications such as dietary fibers, texture modifiers, gelling agents, thickeners, stabilizers, emulsifiers, coatings, films, binders, and encapsulants (Martinetti et al., 2014; Porto and Cristianini, 2014).

This study presents the characterization of the thermal, chemical, and mechanical properties of neem gum. The neem tree, predominantly cultivated in the southern regions of Asia and Africa, has a rich history of use in medical folklore spanning many ages. It belongs to the mahogany family and is characterized as an evergreen plant with a remarkable lifespan exceeding 200 years (Karmakar et al., 2012). Thriving in semi-arid and sub-humid regions, neem is also cultivated in tropical and subtropical climates, flourishing at an annual mean temperature ranging from 21 to 32°C. Successful growth occurs in areas with an annual

E-mail addresses: joymathavan2013@gmail.com, joy@tech.jfn.ac.lk (J.J. Mathavan), mhafizhassan@usm.my (M.H. Hassan).

^{*} Corresponding author.

rainfall below 400 mm, and it exhibits resilience to high temperatures up to 48°C, even in extremely dry conditions (Dhar et al., 2012). However, the plant cannot withstand freezing conditions, particularly during its early growth stages. The neem tree is an evergreen tree that can reach heights of up to 20 m. Adaptable to various soil types, including clay, saline, and alkaline soils with a pH of 8.5, neem can be cultivated directly from seeds or through the transplantation of nursery-raised seedlings with minimal care. It is not preferred by livestock for consumption and is resistant to diseases and pests (Karmakar et al., 2012). Harvestable seeds typically appear within 3–5 years, with full production achievable in a decade, sustaining productivity for up to 150–200 years (Takase et al., 2015). Notably, various parts of the neem tree, such as the leaves, bark, fruit, flowers, oil, and gum, have been associated with traditional medicinal practices for addressing conditions like cancer, hypertension, heart diseases, and diabetes.

Neem gum, a natural, tasteless, amber-colored extrudate obtained from the incised trunk of Azadirachta indica, is a water-soluble, naturally occurring polysaccharide (Asghar et al., 2019; Bhagwat et al., 2020). Native to tropical and semi-tropical regions, this tree consistently produces an abundance of gum throughout the year. Neem gum comprises mannose, glucosamine, arabinose, galactose, fructose, xylose, and glucose (Kalaskar et al., 2021). Neem gum finds diverse applications, particularly in cosmetics and medicines, owing to its water-dispersible, cost-effective, non-toxic, and biocompatible characteristics. The specific chemical groups within neem gum, such as COOH, OH, and CH3CO, contribute to its unique binding capabilities with targeted sites (Asghar et al., 2019). Besides the pharmaceutical industry, the introduction of neem gum to concrete markedly inhibits the corrosion of reinforced steel in NaCl solution (Annaamalai et al., 2018). Further, neem gum has unique properties that can be used as both a bio-electrolyte and a bio-electrode component, exhibiting superior dielectric strength and versatility, suggesting potential utilization in diverse devices (Parangusan et al., 2024). It was also used as bio electrochemical flexible energy storage device (Dhar et al., 2020). The present study addresses a significant research gap by focusing on the thermal, chemical, and mechanical properties of neem gum, which has been relatively unexplored except for its applications in the pharmaceutical sector. Although the few available research papers on neem gum discuss its thermal properties, they lack supporting evidence and verification. The present work provides strong visual evidence of its thermal properties through STA and also verifies the chemical composition of neem gum by FTIR, SEM/EDX, and µ-XRF tests. Furthermore, this is the first time the mechanical properties of neem gum have been analyzed, which will help the academic community and industries to unveil new areas of usage. These facts highlight the novelty and importance of this research.

2. Methodology

2.1. Gum extraction and preparation

Crude neem gum was collected from Azadirachta indica trees manually from northern province of Sri Lanka. This involved the extraction of natural substances that ooze out from the trees. The gum may be dried (Mahfoudhi et al., 2014), dried, ground, and sieved (Nayak et al., 2011), or chopped into bits (Porto and Cristianini, 2014b) before adding water to it. The purpose of these steps is to ensure the purity of gum and to increase the gum polysaccharide's solubility in water (Porto and Cristianini, 2014b). On the other hand, these are not mandatory steps in the extraction and purification procedure if the purity is ensured and solubility is enhanced by any other means (Rincón et al., 2009; Simas-Tosin et al., 2010, 2013). In the current research, the extracted gum was manually cleaned to remove any impurities such as the particles of the bark and other extraneous materials. This step ensures that only the pure exudates are used in the subsequent process. Equal weight of normal water was then added at room temperature (25–30 $^{\circ}\text{C})$ to the cleaned exudates and the mixture was homogenized. This process helps

to achieve a uniform consistency throughout the mixture (Mathavan and Hafiz bin Hassan, 2024). After homogenization, the mixture was left for 24 hours to allow complete dissolution of the exudates in the water. Subsequently, the mixture was filtered using sieve to make sure that no external particles or mucilage were trapped in the gum. This filtration step ensures the purity of the final product. Finally, the filtered mixture was allowed to thicken naturally under ambient temperature and humidity. This allows the gum to achieve the desired consistency suitable for further processing. One portion was then powdered according to the necessity of the thermal and elemental analysis. For mechanical testing, another portion was transferred to a mold with dimensions $20~\mathrm{cm} \times 10~\mathrm{cm}$ with a mold release sheet at the bottom. It was then left to dry naturally in open air at ambient temperature and cut into different sizes based on the tensile, flexural and compressive test requirements.

2.2. Determination of pH

2 g sample of gum was dispersed in sufficient deionized water and the volume was made to 100 ml with more of the deionized water to produce a 2 % $^{\rm w}/_{\rm v}$ dispersion of the polymer. The pH of the dispersion was determined 24 h after preparation using a pH meter provided by EUTECH INSTRUMENTS according to ASTM D1293A standard.

2.3. Thermogravimetric analysis

Most polymers, synthetic or natural, suffer degradation when subjected to thermal stress (Atul and Baldev, n.d). This is attributed to chain depolymerization, point splits, or even the elimination of low molecular weight fragments, which cause mass loss due to the increase in temperature (Crompton, n.d). They cause thermal effects related to physical or chemical changes, and are associated with thermodynamic events (Atul and Baldev, n.d). These changes in energy and mass can be measured by thermogravimetry (TG), derivative thermogravimetry (DTG), differential thermal analysis (DTA) and differential scanning calorimetry (DSC), which make it possible to obtain information such as changes in the crystalline structure, reaction kinetics, melting and boiling point, glass transition, etc. (Michael and Brown, n.d). Thermogravimetry can be defined as changes in mass as a function of temperature and/or time (Wesley William Wendlandt, 1974). It can also be said as continuous registration of mass subjected to heating or cooling (Sesták, 1984).

The TG (thermogravimetric) analysis was performed according to ASTM E1131 standard on a Pyris 1 TGA Thermogravimetric Analyzer supplied by PerkinElmer Life and Analytical Sciences. It has temperature range up to 1000°C , scanning rate of $0.1~^{\circ}\text{C/min}$ - $200~^{\circ}\text{C/min}$, temperature precision of $\pm~2^{\circ}\text{C}$, temperature accuracy of $\pm~0.1~^{\circ}\text{C}$, balance sensitivity of $0.1~\mu g$ and balance precision of 0.001~%. The analyses were carried out on 8.1~mg weighed sample using nitrogen atmosphere with a flow rate of 20~ml/min. The heating rate used was $20~^{\circ}\text{C/min}$, from $30~^{\circ}\text{C}$ to a final temperature of $900~^{\circ}\text{C}$.

2.4. Differential scanning calorimetry

Differential Scanning Calorimetry (DSC) is a robust physical technique employed to track both physical and chemical transformations in polysaccharides during thermal processing, generating distinctive curves for each polysaccharide (Bothara and Singh, 2012). DSC and DTA are analyses that measure energy gradients between the sample and a reference material subjected to controlled temperature. DSC is a calorimetric method in which energy differences are measured, whereas in DTA, temperature differences between the sample and the reference material are registered (Crompton, n.d). DTA provides a qualitative analysis of the thermal events experienced by the sample, whereas DSC is able to quantify such events because it measures the heat flow through a temperature gradient (Müller and Michell, 2016). ASTM D3418 standard is used in this study to perform DSC analysis. DSC Q20 V24.11

equipment from TA instruments was used. It has temperature range up to 725°C, temperature accuracy of \pm 0.1°C, temperature precision of \pm 0.05°C, heating rate up to 200 °C/min, dynamic measurement range of \pm 350 mW and sensitivity of 1 μW . The sample of weight 6.66 mg was used under 50 ml/min nitrogen flow and 10.00 °C/min heat flow until reaching 320°C.

2.5. Simultaneous thermal analysis (STA)

Real time observation of the changes in the sample with increasing temperature is conducted through STA to verify the results obtained from TGA and DSC analysis. Simultaneous thermal analyzer STA8122 manufactured by Rigaku corporation was used under static air to observe and analyze the changes occurring to the sample under ambient environmental conditions. Maximum temperature of 400°C and temperature increasing rate of $20~^{\circ}\text{C/min}$ were preset for testing.

Simultaneous Thermal Analysis (STA) is an analytical technique that concurrently measures both thermogravimetry (TG) and differential thermal analysis (DTA). In thermogravimetry, the analysis involves measuring changes in the sample's weight, enabling the examination of reaction temperatures and the rate of weight change during processes like dehydration, thermal decomposition, evaporation, and oxidation. Differential Thermal Analysis (DTA) is employed to measure endothermic or exothermic reaction temperatures, such as those related to transitions, melting, crystallization, dehydration, decomposition, oxidation, and glass transition temperature. Additionally, STA allows measurements while capturing visual images of the sample using a CCD camera. These images provide valuable insights into shape changes or color variations in the sample associated with a reaction, enhancing the interpretation of STA results. The instrument's capability to combine TG and DTA measurements, along with visual observations, contributes to a comprehensive understanding of thermal events in the analyzed samples.

2.6. Fourier transform infra-red spectrometry (FTIR)

FTIR test according to ASTM E1252 was performed to obtain qualitative infrared spectra of *Azadirachta indica* tree gum. The instrument used for FTIR analysis is 400 Spotlights FTIR Imaging System. It was integrated with Attenuated Total Reflection (ATR) model from PerkinElmer, USA for Mid-NIR infrared analyzing. ATR is an IR sampling technique that provides excellent quality data in conjunction with the best possible reproducibility of any IR sampling technique. The zinc selenide detector is used to detect the spectra transmission with a scan range from $600~{\rm cm}^{-1}$ to $4000~{\rm cm}^{-1}$. The resolution used is 8 cm $^{-1}$ for 16 scans. IR spectrum software version 10.3.2 by PerkinElmer is used to process the spectrum.

2.7. SEM/EDX analysis

Scanning electron microscope (SEM) S-3400 N provided by Hitachi Science Systems, Ltd is used to see the magnified images of the powdered sample. The SEM used has the magnification power from 5x to 300000x, acceleration voltage of 0.3 kV to 30 kV and vacuum pressure of 1.5×10^{-3} Pa. The electron source used is pre-centered cartridge type tungsten hairpin filament. Energy Dispersive X-ray Analysis (EDX) is occupied along with SEM to analyze the elements present in the powdered sample. The sample powder to be imaged is sticked to the sample stage with the help of double-sided adhesive tape and inserted in to the SEM. Once the image is obtained, the EDX is used to scan the image under "area scanning" option to determine the elements present in the specified points of interest. ASTM E 1508 standard is used for the quantitative analysis of SEM/EDX.

2.8. Micro X-ray fluorescence test

Micro X-ray fluorescence (μ -XRF) is the analytical method used in this study according to ASTM E3295 – 23 standards to pinpoint the microscopic elemental makeup of Azadirachta indica tree gum. The μ -XRF used in this work was an M4 Tornado produced by the German company Bruker Nano GmbH in Berlin. Radiation was produced using a rhodium tube. A 40 kV supply with a 600 mA current flow and a 2mbar pressure were used for the experiment. In order to achieve a sharp focus image and a significant amount of X-ray beam scattering, the sample was positioned and adjusted. Based on the photon energy supply from 1.7 keV to 25.5 keV, the μ -XRF used in this work can test metallic samples of thickness 400 nm to 20 μ m, glass, stone or ceramic samples of thickness 4.5 μ m to 3 mm, and plastic or wood samples of thickness 10 μ m to 2 cm.

2.9. Micro hardness

Nano indentation test was conducted to characterize the micro hardness according to ASTM E384, using a Nano Test Vantage machine which was manufactured by Micro Materials Ltd. The experimentation sample should have fine surface finish and should be free from any dirt or grease as these irregularities may affect the readings. Graph of loading and unloading curves and the value of hardness were obtained for further analysis. The nano indentation test consisted of following experiment parameters. Maximum load of 500 mN, minimum load of 50 mN, limit stop load of 0.01 mN, initial load of 0.01 mN, loading and unloading rate of 5.0 mN/s, 6 s dwell at maximum load in one column each containing 10 indentations with Z offset of 0 μ m and Y offset of 15 μ m and retraction distance of 15 μ m.

2.10. Tensile strength

Tensile test (ASTM D638 – 12.7 mm width, 165 mm long and 3.2 mm thickness) was performed on computerized universal testing machine with 400 kN capacity. The tensile test outcomes including tensile strength, strain and young's modulus of the specimen are represented graphically in the results and discussions section. Viknesh Kumar et al. used neem gum powder as the filler material while testing the mechanical properties of the LY 556 Epoxy resin using the same testing method (Kumar et al., 2023). Various other researchers also have used ASTM D638 for tensile test of composite resins (Chandra et al., 2022; Mebratie et al., 2023).

2.11. Flexural strength

Flexural test is performed according to ASTM D790–17 standard. Specimens of thickness 3.2 \pm 0.3 mm, span length of 16 \pm 1 times that of thickness and width less than one forth that of span length is used for the testing (12.7 mm width, 127 mm long, 3.2 mm thickness). Rate of cross head movement was set at 1.5 mm/min and maximum limiting deflection was set at 40 mm. Maximum load, maximum extension, flexural stress, flexural strain and modulus values were obtained from the graph. Some other researchers also have used ASTM D790 for flexural testing of composite resins (Karthikeyan et al., 2022; Nik Wan et al., 2023).

2.12. Compressive strength

ASTM D695 is used to obtain the compressive strength, compressive yield point, and modulus of neem gum. Compression test was conducted on samples of 12.7 mm width, 25.4 mm length and 12.7 mm thickness with a cross-head movement of 1.5 mm/min. The maximum compression specified was 50 % that of the length of the sample. The same UTM machine with different heads was used for each of the tensile, flexural and compression tests.

2.13. Viscosity and electrical resistivity

Viscosity and electrical resistivity were measured within the temperature range of 30°C to 90°C and concentrations of 10, 20, 30 40, and $50~\%^{\text{W}}/_{\text{V}}$ of the gum. The viscosities of the gum dispersions were obtained at different shear rates of 2–100 rpm using Brookfield viscometer version 5 spindle 2 (Brookfield Engineering Labs, Stoughton, USA) according to Eshun et al. (Eshun Oppong et al., 2021). A 3 min standardization was done before the reading of viscosities was taken (Nep and Conway, 2010). In general, viscosity of gums depends on the type of gum, temperature, concentration, pH, and the presence of other substances in the solution. The effect of these individual factors on viscosity varies from gum to gum (Eshun Oppong et al., 2021). A graph of the viscosities against concentration was plotted to evaluate the effect of concentration on viscosity. In this research, multimeter is used to measure the electrical resistance and the resistivity is calculated from the data obtained from it.

3. Results and discussion

3.1. pH value

The pH value obtained for 2 % $^{W}/_{v}$ neem gum was 5.07 \pm 0.02 and which is in the interval between 3.8 and 5.22 as specified by Gyedu-Akoto et al. (Gyedu-Akoto et al., 2008). They further mentioned that, the pH of gums coming from trees of the different age groups and different locations can be vary. Another research group found that the neem gum is acidic in nature (Kalaskar et al., 2021) and it is in the comparable range of khaya gum (pH = 3.38 – 4.2) (Olorunsola et al., 2016), grewia gum (pH = 5.67–5.73) (Nep and Conway, 2010), acacia gum (pH = 4.61) (Olorunsola et al., 2016) and cashew gum (pH = 4.76) (Mathavan and Hafiz bin Hassan, 2024).

3.2. Thermo gravimetric analysis

The process of thermal degradation of polysaccharides starts with random chain scission-related breakdown of the polymerization and ends with molecular rearrangements (Singh and Sharma, 2014). The thermogravimetric curves of neem gum samples are shown in Fig. 1. The first stage up to 116°C is attributed to moisture evaporation with mass loss of 6.44 %. The decomposition of the three biomass lignocellulosic components takes place next. Hemicellulose is the first component to decompose between 168–273°C with mass loss of 9.41 %, followed by cellulose between 279–391°C with mass loss of 43.64 % and the last one is associated with the breaking of the lignin chain of neem gum up to 900°C. At 900°C the residual mass was 16.24 %. These stages were evidenced in the derivative thermo gravimetry (DTG) curve with peak at

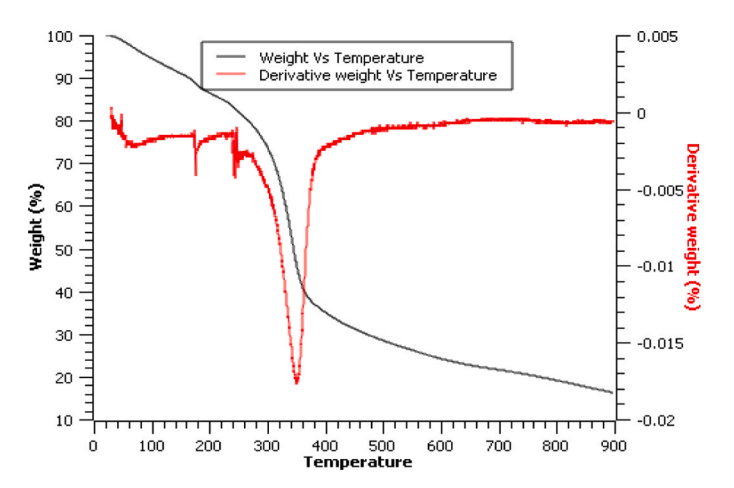


Fig. 1. Thermogravimetric curves obtained for the neem gum sample.

70°C, which is related to moisture removal, and peak at 340°C, which is related to the decomposition of cellulose in neem gum. The derivative of the thermogram, showing the rate of weight change, helps identify specific temperatures at which maximum weight loss occurs. Around 10 % weight loss between 50°C and 120°C because of the elimination of water molecules and a major weight loss of ~47 % at temperature between 210°C to 350°C due to the breaking of the main chains of neem gum was also observed by Asghar et al. (2019). The decomposition of hemicellulose between 200–300°C, followed by cellulose between 250–380°C was also recorded by some researchers for few other biomass lignocellulosic components (Zhou et al., 2013). Samrot et al. also observed a weight loss from 100 % to 63.3 % between the temperature range of 50–485°C for polysaccharide decomposition of neem gum (Samrot et al., 2020).

Cellulose is the compound with the highest activation energies. This is attributed to the fact that the cellulose is a very long polymer of glucose units without any branches (Skreiberg et al., 2011), while hemicellulose has a random branched amorphous structure that gives a lower activation energy; this is the reason why hemicellulose decomposes more easily in a lower temperature range (Chen et al., 2019). Lignin has a very complex structure composed of three kinds of heavily crosslinked phenylpropane structures (Skreiberg et al., 2011) and its decomposition range is the widest (Di Blasi, 2008), occurring from 200°C up to high temperatures such as 900°C. These bonds have relatively high bond energies, requiring more energy input to break them and initiate degradation. Generally, dehydration, depolymerization, decarbonylation and pyrolitic decomposition, with the evolution of H₂O, CO, CO₂, and CH₄ are involved in anionic gum thermal decomposition. However, because of the differences in structure and functional groups, either the degradation routes or the resulting fragments will be different (Cunha et al., 2007).

3.3. Differential scanning calorimetry

Differential scanning calorimetry is a primary technique for measuring the thermal properties of materials to establish a relation between temperature and specific physical properties of materials. The DSC thermograms of the neem gum is shown in Fig. 2. Neem gum sample shows the broad endo (heat absorbs) related peak at 112.1°C and exothermic (heat liberation) peak at 315.3°C respectively. The respective enthalpies associated with these transitions are 479.5 J/g and 53.5 J/g. These findings align with the results of Malviya et al. (Malviya et al., 2018), who reported an endothermic peak at 96°C and an exothermic peak at 300°C for neem gum. Additionally, Bhagwat (Bhagwat et al., 2020) noted a broad endothermic peak at 95.02°C followed by an exothermic peak observed at 303.70°C for neem gum.

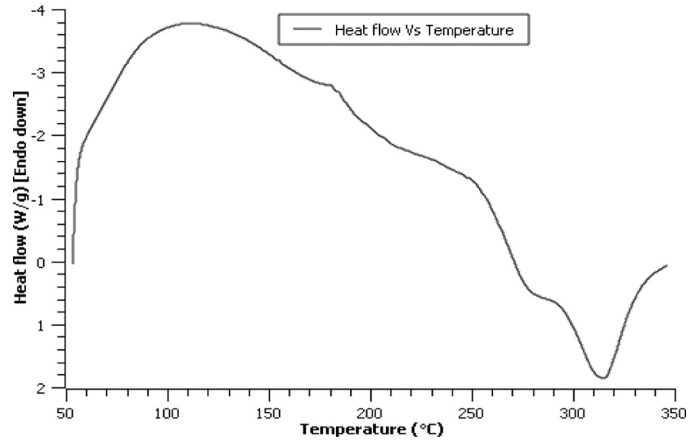


Fig. 2. Differential scanning calorimetry curves obtained for the neem gum sample.

Kalaskar et al. showed that, an endothermic transition between 90°C and 110°C and the peak of it observed at 100°C for the experiments performed on neem gum (Kalaskar et al., 2021).

The broad endothermic transition is attributed to the dehydration of water from the gum, involving the removal of detached water, which can be hydrogen-bonded water, or physically adsorbed water. A broad endothermic peak suggests less regular packing of neem gum (Daoub

et al., 2018a) and a large asymmetric endotherm might be linked to the presence of contaminants (Daoub et al., 2018b; Kumar et al., 2011). In other words, the nonexistence of sharp endothermic peak confirms the amorphous nature of neem gum which is not semi-crystalline in nature. Moreover, many researchers mentioned that the endothermic peaks in the 150 – 231.15 °C temperature range can be attributed to the glass transition of gum polysaccharides (Kamboj and Rana, 2014; Mehetre

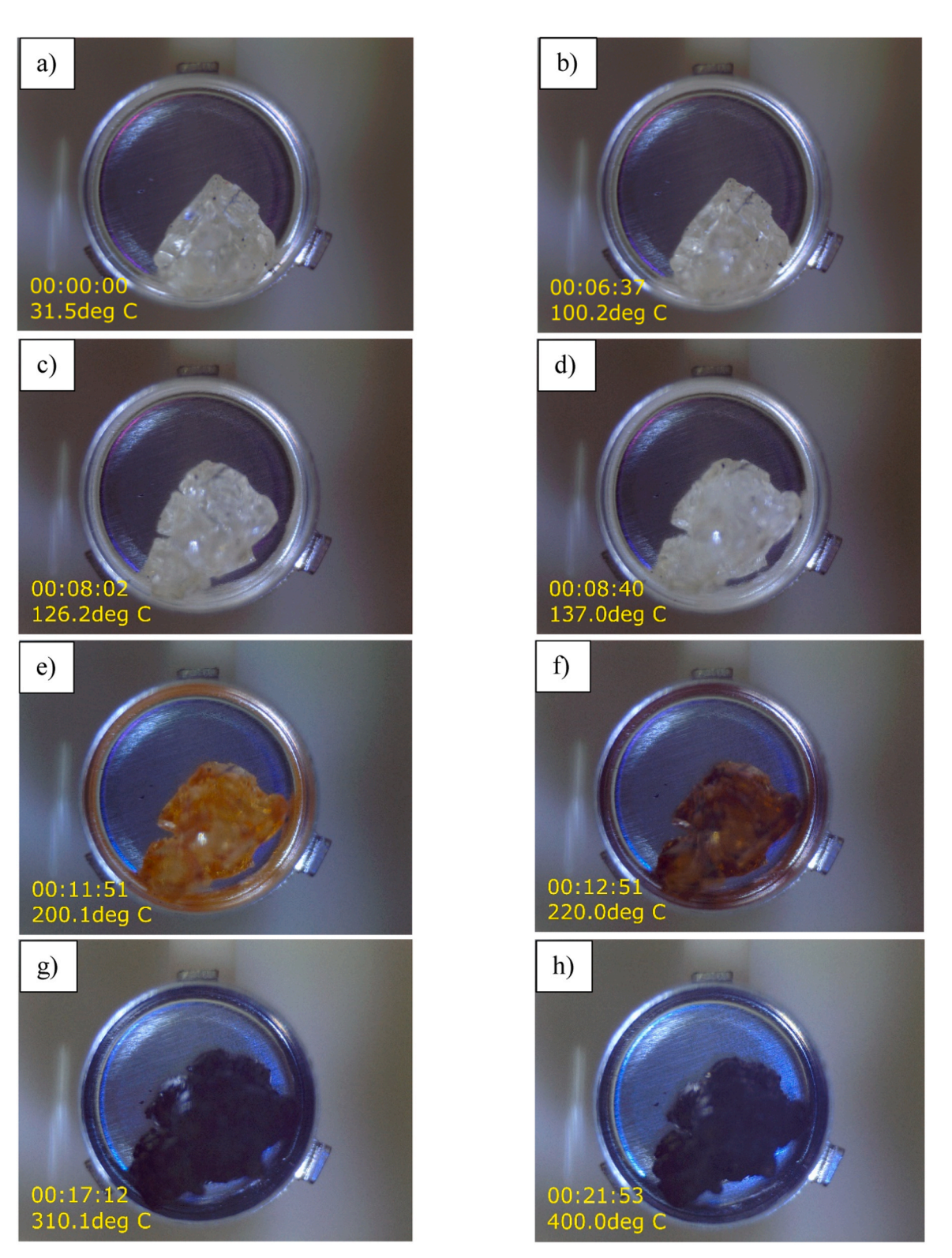


Fig. 3. Images taken at different temperatures (a) first image at start (b) image at 100°C (c) image at the start of first endothermic peak (d) image at the first endothermic peak (e) image at 200°C (f) color change occurring (g) image at first exothermic peak (h) last image at 400°C.

et al., 2015; Nep and Conway, 2010b). The temperature at which a material changes from amorphous or glassy solid state to a viscous rubbery state is known as the glass transition (Tg) (Jasse et al., 1994). The glass transition temperature is higher for plant gum polysaccharides with higher degrees of crystallinity because they have high structural stability (A. K. Singh et al., 2010). Conversely, amorphous gums have lower glass transition temperatures, as found for kondagogu (34.5 °C) (Vinod et al., 2008), tragacanth (74.8 °C) (Martins et al., 2009), Afzelia africana (43.7 °C), and okra (61.5 °C) (M. Emeje et al., 2011). But the present research doesn't signify any endothermic peak within the specified temperature ranges. Therefore, it can be concluded that, the neem gum doesn't have a glass transition temperature and eventually doesn't have a melting point either. 3.4 will further emphasize this fact. There are other plant gums like cashew tree gum which doesn't have a glass transition temperature (Mathavan and Hafiz bin Hassan, 2024). The exothermic peak corresponds to the decomposition of neem gum, involving the breakdown of glycosidic bonds, depolymerization, dehydration, and the formation of stable products such as CO, CO₂, and CH₄ (Jamaludin et al., 2017; Malviva et al., 2018). In the current study, the exothermic transition peak was obtained at 315.3°C and is attributed to the degradation of the polymer as also mentioned by Igbal et al. (Igbal et al., 2013). The observed polysaccharide degradation might be due to high inorganic composition of the polymer (Builders et al., 2008). Similar results have been reported for acacia gum as well (Daoub et al., 2018; Jamaludin et al., 2017).

3.4. Simultaneous thermal analysis (STA)

Certain prominent images of the transformation in STA analysis at different temperatures are shown in Fig. 3. The STA curve exhibits almost similar graphs to that of the individual TGA (3.2) and DSC (3.3) analyses. This concurrence serves to reinforce the previously obtained results and the conclusions drawn from them. The curve distinctly indicates that neem gum undergoes dehydration followed by decomposition upon heating, with no apparent melting point observed. Identification of this phenomena is possible only because the real time changes of neem gum can be observed by the camera fixed within the chamber. Dehydration occurred at the temperature range of 130°C to 150°C and decomposition occurred at the temperature range of 300°C to 330°C as can be seen from Fig. 4. It is also feasible to designate a temperature range on the graph where a swift transformation occurs, enabling the differentiation of phase changes.

3.5. Fourier transform infra-red spectrometry (FTIR)

To discern the chemical bonds within a molecule, Fourier Transform Infrared Spectroscopy (FTIR) is employed to generate the infrared absorption spectrum as shown in Fig. 5. This resulting molecular

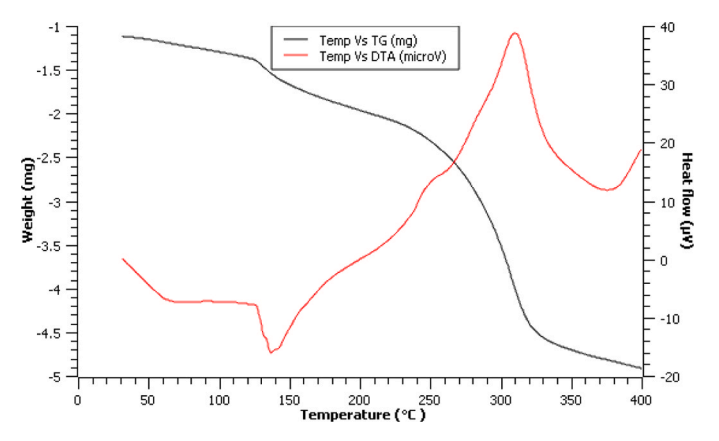


Fig. 4. TG-DTA curve obtained under static air condition.

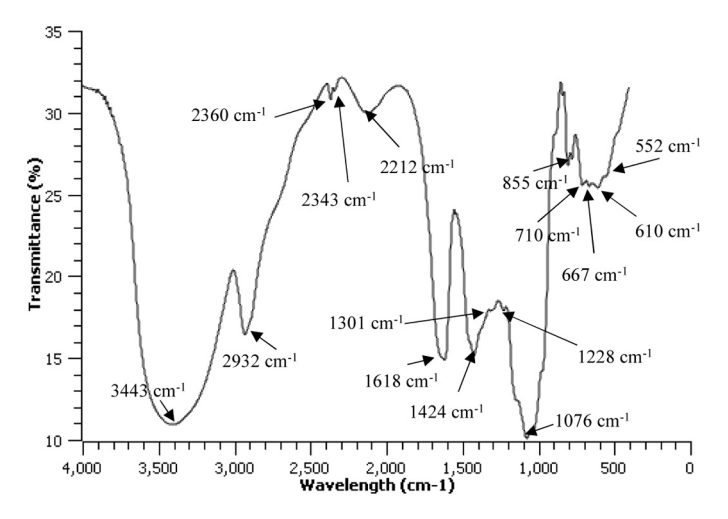


Fig. 5. FTIR spectrum of neem gum.

fingerprint facilitates the examination of various compounds present in the sample. The region spanning 1500-500 cm⁻¹, known as the fingerprint region, is distinctive for each sample, while the region from 4000 to 1500 cm⁻¹ is designated as the functional group region. The neem gum sample tested here was in powder form and added with KBr. The absorption bands and respective functional groups are shown in Table 1. Phadke et al. (2015) and Asghar et al. (2019) also obtained almost similar peaks for pure neem gum. Korkmaz et al. mentioned that, the bands at 1651 cm⁻¹ and 1550 cm⁻¹ indicate the presence of carboxylate, amine and peptide groups in neem gum (Korkmaz et al., 2015). Sakthivel and Mallika expected that, the additional band at $1309~{\rm cm}^{-1}\,{\rm could}$ have arisen from aromatic C-N bond of protein present in the neem gum (Sakthivel and Mallika, 2016). Further, Kamraj et al. anticipated that, the bands at 760 cm⁻¹ and 605 cm⁻¹ could be attributed to the stretching vibration of C-Cl and C-Br bond of alkyl halides present in neem gum (Kamaraj et al., 2018). But the predictions and conclusions made by Korkmaz et al., Kamraj et al., Sakthivel and Mallika could not be supported by the present research because, the neem gum samples tested here didn't show any trace of N, Cl or Br based on the results obtained by the SEM/EDX analysis and micro-X-ray fluorescent analysis. Therefore, the possibility of presence of aromatic C-N bond, the C-Cl and C-Br bond of alkyl halides, and the amine & peptide groups in the neem gum is nullified.

 $\begin{tabular}{ll} \textbf{Table 1} \\ \textbf{Absorption bands and their relevant origin for the graph observed from FTIR} \\ \textbf{Spectrum.} \\ \end{tabular}$

Absorption	Bands (White, 1971)	Origin
3800-3000 cm ⁻¹	Phenolic OH stretching	cellulosic material (Lazzari et al.,
_		2018)
2932 cm^{-1}	CH ₂ asymmetrical	aliphatic bonds (Lazzari et al.,
	stretching	2018)
$2365-2050~{\rm cm}^{-1}$	C≡C bond	hemicellulose and lignin
$1618 \ {\rm cm}^{-1}$	C=C aromatic	lignin sub units (Lazzari et al.,
		2018)
1424 cm^{-1}	CH in-plane deformation	lignin bonds (Xu et al., 2013)
$1301 \; \mathrm{cm}^{-1}$	CH ₂ wagging	Cellulose and hemicellulose (Xu
		et al., 2013)
$1228~{\rm cm}^{-1}$	C-C, C-O stretching	Lignin (Xu et al., 2013)
$1076 \; \mathrm{cm}^{-1}$	C-O stretching vibrations	cellulose and hemicellulose (Xu
	for ester	et al., 2013)
$1030~{\rm cm}^{-1}$	C-O, C=C, C-C-O	cellulose, hemicellulose and lignin
	stretching for alkoxy	(Lazzari et al., 2018)
$870-700 \text{ cm}^{-1}$	Aromatic C-H out of	Hemicellulose (Xu et al., 2013)
	plane bending	
$690-600 \text{ cm}^{-1}$	Aromatic OH out of plane	
	bending	
	-	

3.6. SEM/EDX analysis

Energy Dispersive X-Ray Analysis (EDX), also referred to as Energy Dispersive X-Ray Spectroscopy, serves the purpose of elemental characterization in samples. When high-energy electromagnetic radiations, specifically X-rays, interact with the sample, they cause the ejection of "core" electrons from the atoms, creating holes. Subsequently, these holes are filled by higher-energy electrons, releasing energy in the process. The unique energy released during this phenomenon is distinctive for each element, allowing for identification and quantification of elements present in the sample (Slathia et al., 2021).

In this study, along with higher amount of carbon and oxygen, small amounts of aluminium, magnesium, pottacium and calcium were also found in the neem gum sample. μ -XRF test is also used to support the results (metallic elements) present in the sample. The elements along with their percentage availability is shown in Fig. 6 & 7 and Table 2 & 3. SEM/EDS provides surface analysis, making it suitable for studying surface composition and elemental mapping. This technique is well-suited for elements with low atomic numbers (below 20) because the electron beam can effectively interact with their electronic structures and induce X-ray emissions. SEM/EDX generally has a lower detection limit for light elements, making it more sensitive for the analysis of low atomic number elements. This is particularly advantageous when detecting elements like carbon, nitrogen, oxygen, and fluorine.

3.7. Micro X-ray fluorescence test

It is always a complementary analysis to perform $\mu\text{-XRF}$ along with SEM/EDAX and they are not alternatives to each other. The SEM/EDAX can clearly identify nonmetals and elements which have atomic number less than 20. On the other hand, $\mu\text{-XRF}$ also uses X-rays to excite the sample and measures the emitted characteristic X-rays for element identification. But it is well-suited for elements with higher atomic numbers (above 20) because their X-ray emissions are more prominent and easier to be detected by XRF. XRF generally has a higher detection limit for light elements compared to SEM/EDX. It is more sensitive for elements with higher atomic numbers, such as transition metals and heavy elements. XRF can provide elemental analysis of both the surface and bulk of the sample, making it suitable for studying the overall composition of materials. Table 3.

3.8. Micro hardness

In micro hardness testing, as the indenter pierces into the surface of the materials, they deform and counteract the load applied by the indenter. Thus, Fig. 8 shows the load versus depth curves obtained for

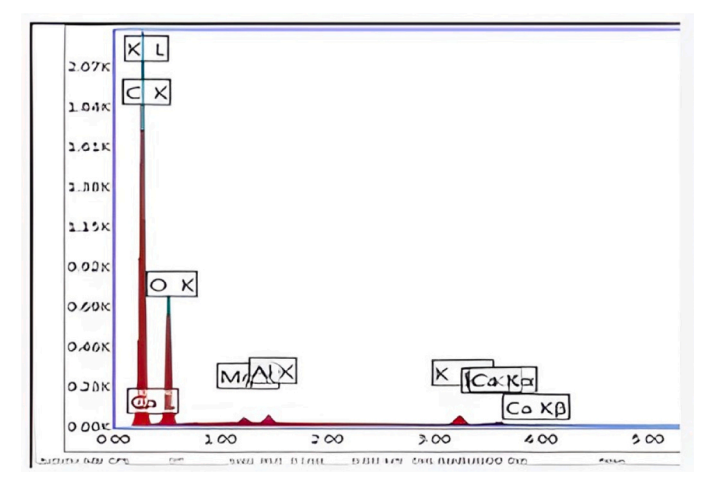


Fig. 6. The constituent elemental spectrum of neem gum using SEM/EDAX.

neem gum during indentation. The maximum depths during the experimental procedure for neem gum samples were around 10230 nm. The hardness value obtained is 238.64 \pm 9 MPa and which is in the comparable range of the experiments performed by Bu et al. on (E51)/furanbased amine curing agents benzene methane-2,2-di (2-furylmethylamine) (BDFA), and epoxy resin (E51)/propane-2,2-di (2-furylmethylamine) (PDFA)) (Bu et al., 2022). E51/PDFA gave 246 \pm 5 MPa and E51/BDFA gave 267 \pm 9 MPa with maximum indentations of 1336 nm and 1281 nm respectively (Bu et al., 2022). Nevertheless, the hardness of neem gum is 1.6 folds less than the hardness of cured poly ester resin (Polyester Resin, 2007).

3.9. Tensile strength

The tensile test is a fundamental mechanical test employed to evaluate the mechanical properties of materials under axial loading. In this test, the specimen is subjected to a gradually increasing axial force until it undergoes deformation and ultimate failure. The variations on ultimate tensile strength and young's modulus for the neem gum specimen were demonstrated in Fig. 9. The ultimate tensile stress of 1.0155 \pm 0.0315 MPa and the maximum variations on percentage of elongation of 9.58 ± 0.813 % was observed during the tensile test as can be seen from Table 4. Usually, plant gums exhibit viscoelastic properties when deformed, meaning they have both viscous and elastic characteristics. There can be different regions identified in tensile test graph such as elastic region, plastic region, ultimate tensile strength (UTS) and fracture point. The initial linear region of the graph (Fig. 9) indicates the elastic region, a measure of the material's stiffness. As the stress increases, the material may enter a plastic region where it continues to deform without a significant increase in stress. This behavior depends on the gum's ductility. UTS indicates the maximum stress the composite can withstand before necking or fracture begins. At last, ductile fracture occurred, which involves significant deformation before failure.

Elongation at break or strain at maximum indicates the material's ductility or ability to deform significantly before breaking. Materials with higher strain at maximum values are considered more ductile. Young's Modulus is a measure of a material's stiffness or rigidity under tensile or compressive loads. It is the ratio of stress to strain within the material's elastic deformation range. A higher young's modulus corresponds to a stiffer material. The tensile strength of neem gum is attributed to hydrogen bonding and molecular interactions that contribute to the formation of the hydration layer around suspended particles, without reducing the surface and interfacial tension

3.10. Flexural strength

Flexural modulus, quantifies the stiffness of a material in response to bending or flexural deformation. The flexural modulus is calculated by analyzing the ratio of stress to strain in the elastic region of the stress-strain curve obtained from a flexural test. The flexural strength, flexural extension, flexural strain and flexural modulus at maximum flexural load of 4.52 \pm 0.776 N were 1.899 \pm 0.304 MPa, 2.57 \pm 0.487 mm, 0.0134 \pm 0.0036 and 248 \pm 17.27 MPa respectively as demonstrated in Table 5.

Flexural stress at maximum load often referred to as modulus of rupture (MOR) or bending strength, is the highest stress experienced by the material on the tension side during a flexural test. It indicates the material's ability to withstand bending stresses and is crucial for designing components subjected to bending loads. Flexural extension at maximum load is the measure of how far a material extends or deforms in its stretched state during a flexural test. This parameter emphasizes the material's ductile behavior under bending stresses. Atomic Young's Modulus is a measure of the stiffness of individual atoms or atomic-scale structures within a material. This parameter is more relevant to the microscopic or atomic-level understanding of a material's response to bending. It reflects the inherent stiffness of material at the atomic scale.

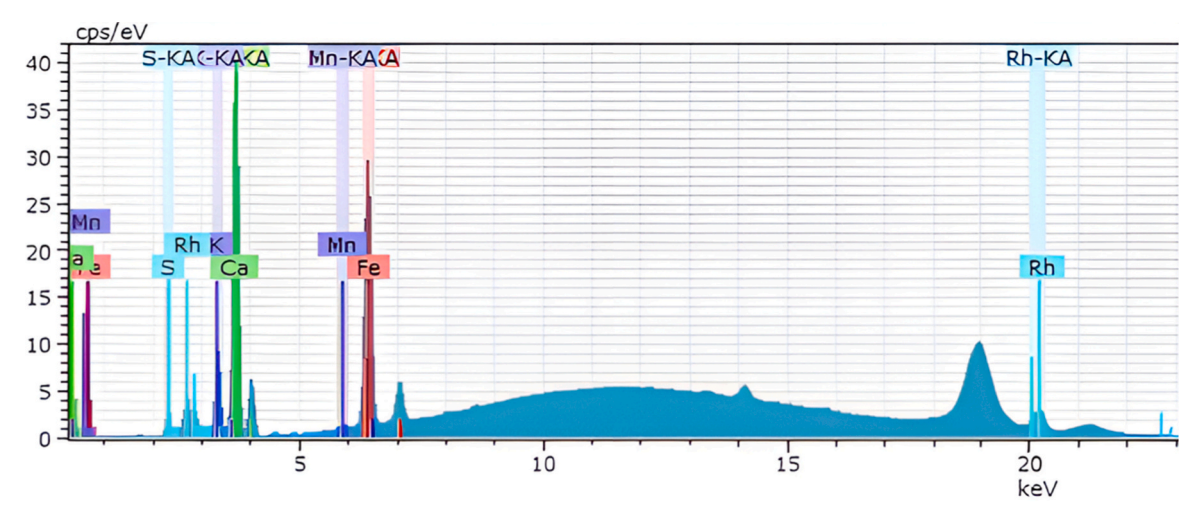


Fig. 7. μ-XRF Spectrum obtained for neem gum.

 Table 2

 Elements observed in neem gum using SEM/EDAX.

Element	Weight (%)	Atomic (%)
С	45.65	53.7
0	50.34	44.53
Mg	0.52	0.3
Al	0.76	0.4
K	1.97	0.71
Ca	0.76	0.27

Table 3 Elements observed in neem gum using μ -XRF.

Element	Atomic Number	[wt%]	[norm. wt %]	Error in wt% (1 Sigma)
Iron	26	1.749346	20.46532	0.001384
Calcium	20	5.151819	60.27031	0.003796
Potassium	19	1.290836	15.10129	0.002113
Sulfur	16	0.323442	3.783896	0.001047
Manganese	25	0.032412	0.379184	0.000209
		8.547855	100	

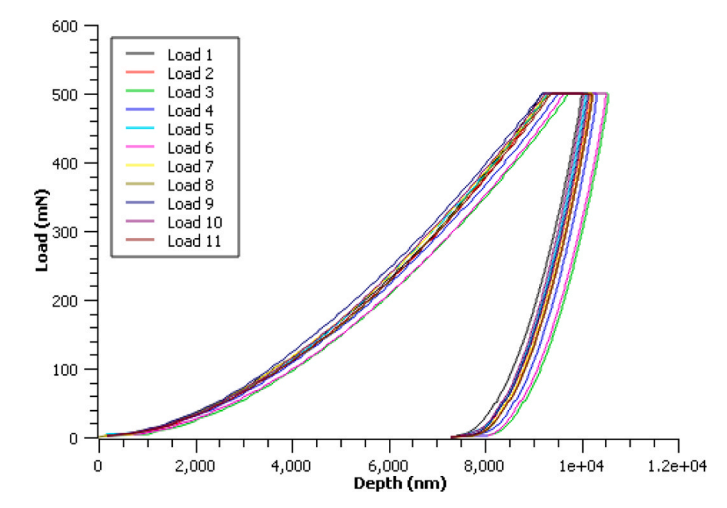


Fig. 8. Loading and unloading curves obtained for neem gum for micro hardness testing.

Flexural strain at maximum load represents the maximum amount of deformation or bending that a material undergoes before it fails in a flexural test. It provides insight into the material's ability to bend or flex under load and indicates its ductility in response to bending stresses. The graph of flexural strength Vs load is shown in Fig. 10. Since neem gum is amorphous in nature, it tends to exhibit more ductile behavior with higher strain. The variation of the flexural strength can be attributed to the molecular sizes of the gum since it contains macromolecules. Uneven distribution of these macromolecules may lead to variations in the density of the gum, creating regions with different physical properties. Usually, a more uniform particle size distribution typically leads to more consistent mechanical properties. Since it dried under ambient conditions, uneven drying or improper curing might have also led to internal stresses and variations in flexural stress and strain. Uneven drying creates moisture gradients within the gum. The outer layers dry faster than the inner layers, leading to differential shrinkage. These gradients generate tensile and compressive stresses within different regions of the gum. The outer, drier layers may shrink and contract, while the inner, wetter layers resist this contraction. This can lead to areas of high stress concentration, increasing the risk of cracks while flexural loading.

3.11. Compressive strength

Compression test is a mechanical testing method used to assess the ability of a material to withstand axial loads that tend to compress it. During compression test, the specimen is subjected to a compressive force along its longitudinal axis, inducing deformation. The variation of the composite specimen's compressive load Vs compressive extension is shown in Fig. 11 (a) and compressive strength Vs compressive strain were demonstrated in Fig. 11 (b). The data indicates that the stress strain relationship is linear in the region below 120 N and obeys Hooke's law. When the stress is released in this area, the material deforms elastically and will return to its initial length. The yield point, (at around 150 N compressive load) is where this linear area ends. Beyond this threshold, the material exhibits plastic behavior and, if the stress is released, will not revert to its initial length. The maximum compressive strength of 1.1023 \pm 0.138 MPa and compressive strain of 0.46 \pm 0.0191, was obtained for neem gum as can be seen from Table 6. Compressive strength is the maximum stress a material can withstand before failure in compression. Compressive strain represents the amount of deformation or strain the material undergoes before reaching failure under compression. 189.96 \pm 8.497 N was the maximum load applied for 50 % compression of the specimen. The variation in the compressive strength may be attributed to the presence of internal voids, or cracks. Surface imperfections and the orientation of polymer chains within the

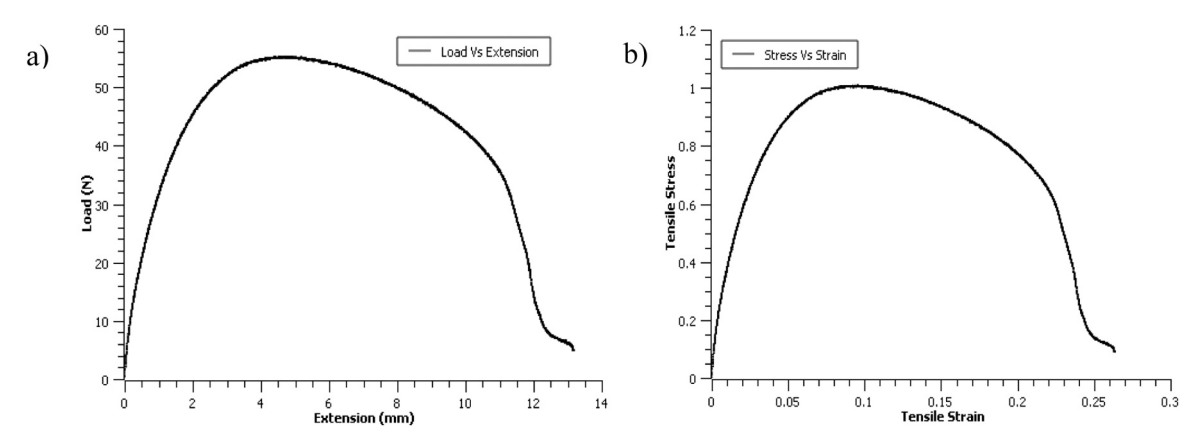


Fig. 9. (a) Load Vs extension and (b) Stress Vs strain graphs obtained under tensile test.

Table 4
Results obtained from tensile test.

Strain at maximum	Stress at maximum	Young's Modulus
(%) 9.582 ± 0.813	(MPa) 1.0155 ± 0.0315	(MPa) 49.405 ± 7.849

Table 5Results obtained from flexural test.

Maximum Flexure load	Flexure extension at Maximum Flexure load	Flexure strain at Maximum Flexure load	Flexure stress at Maximum Flexure load	Modulus (Automatic Young's)
(N)	(mm)	(mm/mm)	(MPa)	(MPa)
4.5237033	2.577088333	0.013491667	1.899503333	248.753163
± 0.776	± 0.487	± 0.0036	± 0.304	± 17.27

gum could also have acted as stress concentrators, impacting the compressive strength response. When polymer chains are aligned in the direction of the applied load, they can more effectively distribute the stress along the length of the chains. This alignment typically enhances the compressive strength, because the load is shared among multiple chains. In materials with randomly oriented chains, the load distribution is less efficient. The stress is unevenly distributed, and fewer chains are aligned in the direction that can support the load, leading to variation in compressive strength.

3.12. Viscosity

Fig. 12 shows the decrease in viscosity with increasing temperature, which is a common phenomenon observed in many liquids and is primarily attributed to changes in molecular motion. As the temperature rises, the kinetic energy of the liquid molecules also increases. This increased kinetic energy leads to greater molecular movement and weaker intermolecular forces. Consequently, the molecules become more mobile and can slide past each other more easily. Viscosity is a measure of a fluid's resistance to deformation or flow. At higher temperatures, the enhanced molecular motion disrupts the organized structure of the liquid, reducing internal friction and making the liquid less resistant to flow. Additionally, the weakening of intermolecular forces reduces the cohesive forces between molecules, further contributing to the decline in viscosity. Further, the viscosity increases with the increase in the concentration of neem gum in the solution as well. Natural plant gums often contain large, complex polymers. When these polymers are present at higher concentrations, they have a greater tendency to become entangled with each other. This entanglement restricts the movement of individual polymer chains, leading to an increase in viscosity. Also, at higher concentrations, there is a greater chance for intermolecular interactions, such as hydrogen bonding, between the polymer chains. These interactions contribute to the overall structural integrity of the gum solution, making it more resistant to flow. Understanding and controlling the viscosity of plant gum solutions is important in various industries, such as food, cosmetics, and pharmaceuticals, where these natural polymers are commonly used as thickeners, stabilizers, or gelling agents.

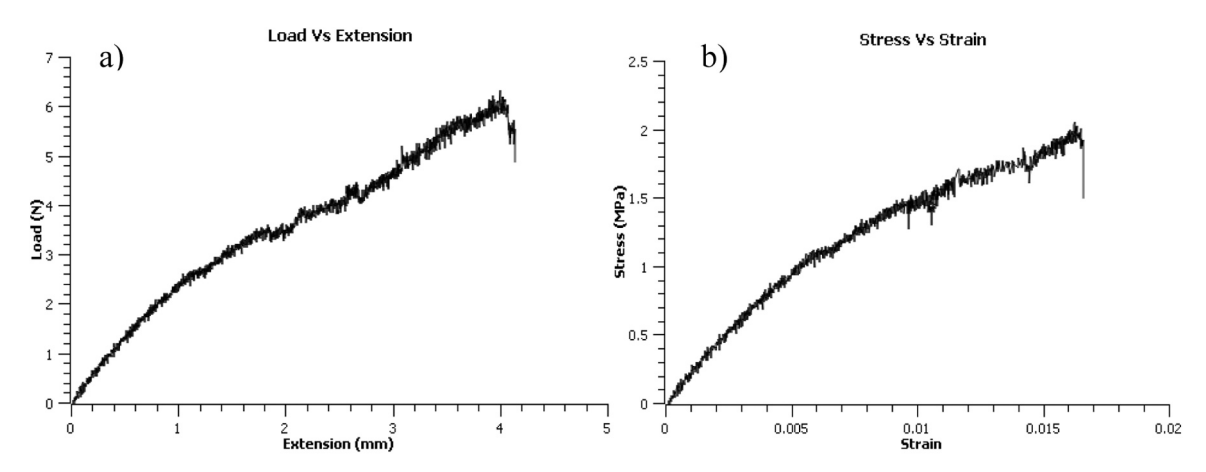
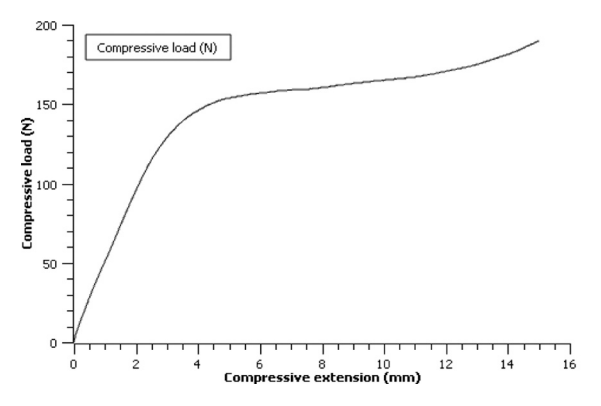


Fig. 10. (a) Load Vs extension and (b) Stress Vs strain graphs obtained under flexural test.



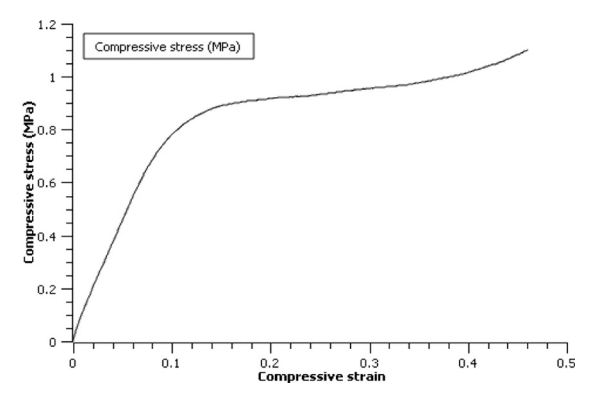


Fig. 11. (a) Load Vs extension and (b) Stress Vs strain graphs obtained under tensile test.

Table 6Results obtained from compression test.

Maximum Compressive load (N)	Compressive extension at Maximum Compressive load (mm)	Compressive strain at Maximum Compressive load	Compressive stress at Maximum Compressive load (MPa)
189.96423 ± 8.497	14.990018 ± 0.021	$\begin{array}{c} \textbf{0.460546} \; \pm \\ \textbf{0.0191} \end{array}$	1.102332 ± 0.138

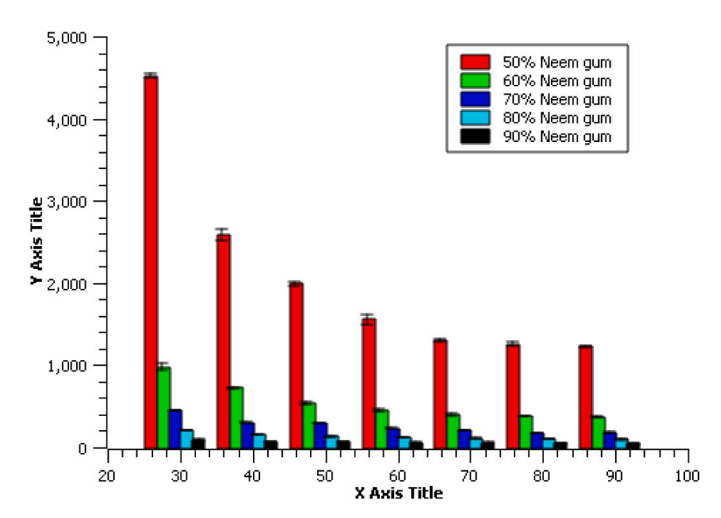


Fig. 12. Viscosity variation of neem gum with increasing temperature and % neem gum mixture.

3.13. Electrical resistivity

The electrical resistivity of the gum was plotted against the temperature and concentration of the gum as can be seen from Fig. 13. According to the graph, the electrical resistivity decreases with increase in concentration and increase in temperature. Since the ions in the neem gum sample are the charge carriers, the increase in concentration of it reduce the electrical resistivity because high amount of charge carriers support conductivity. When the temperature of the solution increases, the kinetic energy of the molecules in the solution also increases. This higher kinetic energy facilitates greater mobility of ions within the solution, which in turn contributes to electrical conductivity. Therefore, an increase in temperature allows ions to move more freely, leading to a decrease in electrical resistivity.

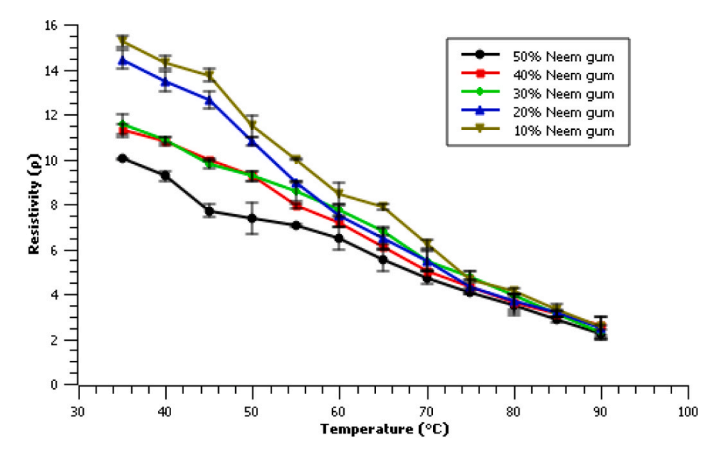


Fig. 13. Change of electrical resistivity of neem gum with temperature and concentration.

4. Conclusion

The comprehensive analysis conducted on neem gum reveals valuable insights into its thermal, chemical and mechanical properties. The findings from various analytical techniques provide a multifaceted understanding of this natural polymer. The pH value of neem gum is 5.07. TGA exposes the thermal behavior of neem gum, with distinct stages corresponding to moisture evaporation and the decomposition of hemicellulose, cellulose, and lignin. The decomposition profile provides essential information for understanding the thermal stability of neem gum. DSC analysis elucidates the thermal transitions of neem gum, showcasing endothermic peaks related to dehydration and exothermic peaks associated with polymer degradation. The absence of sharp endothermic peaks indicates the amorphous nature of neem gum, which in other words doesn't have a crystal structure. Due to this reason, it doesn't have a melting point as proved by STA analysis. FTIR spectra highlights the key absorption bands, revealing the presence of various functional groups in neem gum. The interpretation of absorption bands assists in identifying specific chemical bonds, providing a molecular fingerprint for the gum. Surface analysis through SEM/EDAX and μ-XRF unveils the elemental composition of neem gum, emphasizing the presence of carbon, oxygen, and small amount of other elements like aluminum, magnesium, potassium, and calcium. When considering the mechanical properties, the micro hardness test indicates 238.64 MPa as the hardness of neem gum, and the obtained value aligns with comparable studies on resin materials. Further, the tensile strength, flexural strength and compressive strength of neem gum are 1.0155 MPa, 1.899 MPa and 1.1023 MPa respectively. The combined results from these analyses offer a comprehensive understanding of neem gum, providing valuable data for researchers and industries exploring its

applications in various fields. The diverse range of analytical techniques contributes to a thorough characterization of neem gum from thermal, chemical and mechanical perspectives. Further comparison with synthetic resins may lead to replace synthetic resins with neem gum in various day to day applications.

Comparing the results obtained in this study with the properties of artificial resins in the future may provide valuable insights into the similarities and differences between natural and synthetic resins. This comparative analysis is expected to understand the characteristics of neem gum and explore its potential applications. Neem gum is already been used in pharmaceutical industry. It can also be used as a cap to cutting tools like drill bits (after manufacturing) during transportation to protect its sharp edges being vulnerable to any damages. Further analysis may also yield a path for the application of neem gum as a binding agent or matrix while using it in adhesive industries. It can also be used as electrical insulations since it has a higher resistivity under low temperature. But there is always a critical temperature above which conductivity will reduce and thereby enhance the resistivity due to restriction in the mobility of ions beyond critical temperature. This critical temperature needs to be explored in the future.

CRediT authorship contribution statement

Joy Mathavan: Writing – original draft, Methodology, Formal analysis, Conceptualization. **Muhammad Hafiz Bin Hassan:** Writing – review & editing, Supervision, Investigation, Conceptualization.

Disclosure

The authors declare that they have no known competing financial interests or personal relationships that could have appeared to influence the work reported in this paper.

Formatting of funding sources

This research did not receive any specific grant from funding agencies in the public, commercial, or not-for-profit sectors.

Declaration of Competing Interest

The authors declare that they have no known competing financial interests or personal relationships that could have appeared to influence the work reported in this paper.

Data availability

No data was used for the research described in the article.

Acknowledgement

The authors would like to thank the facility and technical support from the School of Mechanical Engineering, Universiti Sains Malaysia and Department of Biosystems Technology, University of Jaffna.

Appendix A. Supporting information

Supplementary data associated with this article can be found in the online version at doi:10.1016/j.jallcom.2024.175973.

References

Annaamalai, M.G.L., Maheswaran, G., Ramesh, N., Kamal, C., Venkatesh, G., Vennila, P., 2018. Investigation of corrosion inhibition of welan gum and neem gum on reinforcing steel embedded in concrete. Int. J. Electrochem. Sci. 13 (10), 9981–9998. https://doi.org/10.20964/2018.10.41.

- Asghar, K., Qasim, M., Das, D., 2019a. Synthesis and characterization of neem gum coated superparamagnetic nanoparticle based novel nanobiocomposite. Ceram. Int. 45 (18), 25069–25077. https://doi.org/10.1016/j.ceramint.2019.04.050.
- Atul Tiwari; Baldev Raj. (n.d). Reactions and Mechanisms in Thermal Analysis of Advanced Materials. Scrivener Publishing LLC. https://doi.org/10.1002/9781119117711.
- Bhagwat, D.A., Kolekar, V.R., Nadaf, S.J., Choudhari, P.B., More, H.N., Killedar, S.G., 2020. Acrylamide grafted neem (Azadirachta indica) gum polymer: screening and exploration as a drug release retardant for tablet formulation. Carbohydr. Polym. 229 (September 2019)) https://doi.org/10.1016/j.carbpol.2019.115357.
- Bothara, S.B., Singh, S., 2012. Thermal studies on natural polysaccharide. Asian Pac. J. Trop. Biomed. 2 (2, Supplement), S1031–S1035. https://doi.org/10.1016/S2221-1691(12)60356-6.
- Bu, M., Zhang, X., Zhou, T., Lei, C., 2022. Fully bio-based epoxy resins derived from magnolol and varying furan amines: cure kinetics, superior mechanical and thermal properties. Eur. Polym. J. 180, 111595 https://doi.org/10.1016/j. eurpolymi.2022.111595.
- Builders, P.F., Kunle, O.O., Adikwu, M.U., 2008. Preparation and characterization of mucinated agarose: a mucin-agarose physical crosslink. Int. J. Pharm. 356 (1–2), 174–180. https://doi.org/10.1016/j.ijpharm.2008.01.006.
- Chandra, T.O., Sentanu, D.A., Gornes, W., Sentanuhady, J., Setiawan, A., Santos, G.N., Muflikhun, M.A., 2022. Tensile properties of epoxy resin filled with activated carbon derived from coconut shell. Mater. Today.: Proc. 66, 2967–2971. https://doi.org/ 10.1016/j.matpr.2022.06.568.
- Chen, W.-H., Wang, C.-W., Ong, H.C., Show, P.L., Hsieh, T.-H., 2019. Torrefaction, pyrolysis and two-stage thermodegradation of hemicellulose, cellulose and lignin. Fuel 258, 116168. https://doi.org/10.1016/j.fuel.2019.116168.
- Choudhary, S., Sharma, K., Mishra, P.K., Kumar, V., Sharma, V., 2023. Development and characterization of biodegradable agarose/gum neem/nanohydroxyapatite/polyoxyethylene sorbitan monooleate based edible bio-film for applications towards a circular economy. Environ. Technol. Innov. 29, 103023 https://doi.org/10.1016/j.eti.2023.103023.
- T.R. Crompton. (n.d). Thermal Methods of Polymer Analysis. Smithers Rapra Technology. Cunha, P.L.R., Maciel, J.S., Sierakowski, M.R., De, Paulaa, R.C.M., Feitosa, J.P.A., 2007. Oxidation of cashew tree gum exudate polysaccharide with TEMPO reagent. J. Braz. Chem. Soc. 18 (1), 85–92. https://doi.org/10.1590/S0103-50532007000100009.
- Daoub, R.M.A., Elmubarak, A.H., Misran, M., Hassan, E.A., Osman, M.E., 2018a. Characterization and functional properties of some natural Acacia gums. J. Saudi Soc. Agric. Sci. 17 (3), 241–249. https://doi.org/10.1016/j.jssas.2016.05.002.
- Daoub, R.M.A., Elmubarak, A.H., Misran, M., Hassan, E.A., Osman, M.E., 2018b. Characterization and functional properties of some natural Acacia gums. J. Saudi Soc, Agric, Sci. 17 (3), 241–249. https://doi.org/10.1016/j.jssas.2016.05.002.
- Dhar, A., Kevin, R., Agarwal, A.K., 2012. Production of biodiesel from high-FFA neem oil and its performance, emission and combustion characterization in a single cylinder DICI engine. Fuel Process. Technol. 97, 118–129. https://doi.org/10.1016/j. fuproc.2012.01.012.
- Dhar, A., Kumar, N.S., Khimani, M., Al-Fatesh, A.S., Ibrahim, A.A., Fakeeha, A.H., Bhadja, P., Vekariya, R.L., 2020. Naturally occurring neem gum: an unprecedented green resource for bioelectrochemical flexible energy storage device. Int. J. Energy Res. 44 (2), 913–924. https://doi.org/10.1002/er.4949.
- Di Blasi, C., 2008. Modeling chemical and physical processes of wood and biomass pyrolysis. Prog. Energy Combust. Sci. 34 (1), 47–90 https://doi.org/https://doi.org/10.1016/j.pecs.2006.12.001.
- Emeje, M., Isimi, C., Byrn, S., Fortunak, J., Kunle, O., Ofoefule, S., 2011. Extraction and physiochemical characterization of a new polysaccharide obtained from the fresh fruits of Abelmoschus esculentus. Iran. J. Pharm. Res. 10 (2), 237–246.
- Eshun Oppong, E., Kuntworbe, N., Asantewaa Osei, Y., Ofori-Kwakye, K., Adi-Dako, O., Obese, E., 2021. Physicochemical characterisation of Piptadeniastrum africana (Hook. F.) gum, a potential pharmaceutical excipient. Sci. Afr. 13, e00925 https://doi.org/10.1016/j.sciaf.2021.e00925.
- Gyedu-Akoto, E., Oduro, I., Amoah, F.M., Oldham, J.H., Ellis, W.O., Opoku-Ameyaw, K., Hakeem, R.B., 2008. Physico-chemical properties of cashew tree gum. Afr. J. Food Sci. 2 (2), 60–64.
- Iqbal, M.S., Massey, S., Akbar, J., Ashraf, C.M., Masih, R., 2013. Thermal analysis of some natural polysaccharide materials by isoconversional method. Food Chem. 140 (1–2), 178–182. https://doi.org/10.1016/j.foodchem.2013.02.047.
- Jamaludin, J., Adam, F., Rasid, R.A., Hassan, Z., 2017. Thermal studies on Arabic gum-carrageenan polysaccharides film. Chem. Eng. Res. Bull. 19, 80–86. https://doi.org/10.3329/cerb.v19i0.33800.
- Jasse, B., Seuvre, A.M., M. M, 1994. Permeability and structure in polymeric packaging materials. In: Mathlouthi, M. (Ed.), Food Packaging and Preservation. Springer US, pp. 1–22. https://doi.org/10.1007/978-1-4615-2173-0_1.
- Kalaskar, M.G., Mutha, R.E., Tatiya, A.U., Firke, S.D., Surana, S.J., Dhoka, K.A., Heda, K., 2021. Purification and modification of neem gum for enhancement of its suspending property. Future J. Pharm. Sci. 7 (1) https://doi.org/10.1186/s43094-021-00265-9.
- Kamaraj, C., Gandhi, P.R., Elango, G., Karthi, S., Chung, I.-M., Rajakumar, G., 2018. Novel and environmental friendly approach; impact of Neem (Azadirachta indica) gum nano formulation (NGNF) on Helicoverpa armigera (Hub.) and Spodoptera litture (Fab.). Int. J. Biol. Macromol. 107, 59–69. https://doi.org/10.1016/j. iibiomac. 2017.08 145.
- Kamboj, S., Rana, V., 2014. Physicochemical, rheological and antioxidant potential of corn fiber gum. Food Hydrocoll. 39, 1–9. https://doi.org/10.1016/j. foodhyd.2013.12.015.
- Karmakar, A., Karmakar, S., Mukherjee, S., 2012. Biodiesel production from neem towards feedstock diversification: Indian perspective. Renew. Sustain. Energy Rev. 16 (1), 1050–1060. https://doi.org/10.1016/j.rser.2011.10.001.

- Karthikeyan, R., Girimurugan, R., Sahoo, G., Maheskumar, P., Ramesh, A., 2022. Experimental investigations on tensile and flexural properties of epoxy resin matrix waste marble dust and tamarind shell particles reinforced bio-composites. Mater. Today.: Proc. 68, 2215–2219. https://doi.org/10.1016/j.matpr.2022.08.435.
- Korkmaz, F., Erdogan, D.A., Özalp-Yaman, 2015. Interaction of a novel platinum drug with bovine serum albumin: FTIR and UV-Vis spectroscopy analysis. N. J. Chem. 39 (7), 5676–5685. https://doi.org/10.1039/C5NJ00785B.
- Kumar, G., Battu, G.R., Kotha, N., Raju, L., 2011. Isolation and evaluation of tamarind seed polysaccharide being used as a polymer in pharmaceutical dosage forms. Res. J. Pharma. Biol. Chem. Sci. 2, 274–290 https://api.semanticscholar.org/CorpusID: 39727473
- Kumar, M.G.V., Bharathiraja, G., Karunagaran, N., Muniappan, A., 2023. Experimental investigation of Azadirachta indicagum blended bio-polymer composite. Mater. Today.: Proc. 80 (xxxx), 2773–2776. https://doi.org/10.1016/j.matpr.2021.07.036.
- Kurt, A., Cengiz, A., Kahyaoglu, T., 2016. The effect of gum tragacanth on the rheological properties of salep based ice cream mix. Carbohydr. Polym. 143, 116–123. https:// doi.org/10.1016/j.carbpol.2016.02.018.
- Lazzari, E., Schena, T., Marcelo, M.C.A., Primaz, C.T., Silva, A.N., Ferrão, M.F., Bjerk, T., Caramão, E.B., 2018. Classification of biomass through their pyrolytic bio-oil composition using FTIR and PCA analysis. Ind. Crops Prod. 111, 856–864. https://doi.org/10.1016/j.indcrop.2017.11.005.
- Mahfoudhi, N., Sessa, M., Chouaibi, M., Ferrari, G., Donsì, F., Hamdi, S., 2014.
 Assessment of emulsifying ability of almond gum in comparison with gum arabic using response surface methodology. Food Hydrocoll. 37, 49–59. https://doi.org/10.1016/j.foodhyd.2013.10.009.
- Malviya, R., Sharma, P.K., Dubey, S.K., 2018. Stability facilitation of nanoparticles prepared by ultrasound assisted solvent-antisolvent method: effect of neem gum, acrylamide grafted neem gum and carboxymethylated neem gum over size, morphology and drug release. Mater. Sci. Eng.: C. 91, 772–784. https://doi.org/ 10.1016/j.msec.2018.06.013.
- Martinetti, L., Mannion, A.M., Voje, W.E., Xie, R., Ewoldt, R.H., Morgret, L.D., Bates, F.S., Macosko, C.W., 2014. A critical gel fluid with high extensibility: the rheology of chewing gum. J. Rheol. 58 (4), 821–838. https://doi.org/10.1122/1.4874322.
- Martins, E.O., Omoyeme, I., Christiana, I., Ofoefule, S.I., Olobayo, K.O., 2009. Isolation, characterzation and compaction properties of Afzelia africana gum exudates in hydrochlorothiazide tablet formulations. African J. Pharm. Pharmacol. 3, 265–272 https://api.semanticscholar.org/CorpusID:56567295.
- Mathavan, J.J., Hafiz bin Hassan, M., 2024. Thermal chemical mechanical characterization of Anacardium occidentale tree gum. Int. J. Biol. Macromol., 132396 https://doi.org/10.1016/j.ijbiomac.2024.132396.
- Mebratie, B.A., Ayele, B.S., Meku, A.A., 2023. Investigating the tensile and flexural strength of sunflower oil treated Ethiopian Highland bamboo fibre reinforced polyester composites. Adv. Bamboo Sci., 100021 https://doi.org/10.1016/j. bamboo.2023.100021.
- Mehetre, G., Pande, V., Kendre, P., 2015. Isolation and characterization of bionanofibers from *Moringa oleifera* gum as a platform for drug delivery. Nanosci. Nanotechnol. Res. 3 (1), 1–5 https://doi.org/10.12691/nnr-3-1-1.
- Michael E., Brown, P.K.G. (n.d). Introduction to recent advances, techniques and applications of thermal analysis and calorimetry. In P. K. G. Michael E. Brown (Ed.), Handbook of Thermal Analysis and Calorimetry (1st Editio, pp. 1–12). Elsevier B.V.
- Mirhosseini, H., Amid, B.T., 2012. A review study on chemical composition and molecular structure of newly plant gum exudates and seed gums. Food Res. Int. 46
- (1), 387–398. https://doi.org/10.1016/j.foodres.2011.11.017.
 Müller, A.J., Michell, R.M., 2016. Differential scanning calorimetry of polymers. Polym. Morphol. 72–99. https://doi.org/10.1002/9781118892756.ch5.
- Nayak, R.K., Patil, S.R., Patil, M., Bhat, M., 2011. Evaluation of disintegrating properties of Mangifera indica gum. RGUHS J. Pharm. Sci. 1 (1), 11–20.
- Nep, E.I., Conway, B.R., 2010a. Characterization of Grewia Gum, a potential pharmaceutical excipient. J. Excip. Food Chem. 1 (1), 30–40.
- Nep, E.I., Conway, B.R., 2010b. Characterization of Grewia Gum, a potential pharmaceutical excipient. J. Excip. Food Chem. 1 (1), 30–40.
- Nik Wan, F., AbuBakar, A., Suriani, M.J., Saat, A.M., Fitriadhy, A., Wan Nik, W.B., Abdul Majid, M.S., Mukhtar, Z.Z., 2023. The flexural properties of oil palm trunk (OPT) impregnated with epoxy (OPTE) composite manufactured by vacuum-assisted resin transfer moulding (VARTM) technique. Eng. Fail. Anal. 147, 107127 https://doi.org/10.1016/j.engfailanal.2023.107127.
- Nussinovitch, Amos, 2009. Plant Gum Exudates of the World Sources, Distribution, Properties, and Applications (1st Editio. CRC Press. https://doi.org/10.1201/ 9781420052244
- Olorunsola, E.O., Bhatia, P.G., Tytler, B.A., Adikwu, M.U., 2016. Thermochemical properties of hydrophilic polymers from cashew and khaya exudates and their

- implications on drug delivery. J. Drug Deliv. 2016, 1–7. https://doi.org/10.1155/2016/7496585.
- Parangusan, K., Subramaniam, V., babu, A., venkatesh, P.S., Vijayalakshmi, S., Ponnamma, D., 2024. Biocompatible neem gum-modified polyvinyl alcohol composite as dielectric material for flexible energy devices. Heliyon 10 (7), e28379. https://doi.org/10.1016/j.heliyon.2024.e28379.
- Phadke, C., Mewada, A., Dharmatti, R., Thakur, M., Pandey, S., Sharon, M., 2015. Biogenic synthesis of fluorescent carbon dots at ambient temperature Using Azadirachta indica (Neem) gum. J. Fluoresc. 25 (4), 1103–1107. https://doi.org/ 10.1007/s10895-015-1598-x
- Polyester Resin. (2007). Hawley's Condensed Chemical Dictionary. https://doi.org/10.1
- Porto, B.C., Cristianini, M., 2014b. Evaluation of cashew tree gum (Anacardium occidentale L.) emulsifying properties. LWT Food Sci. Technol. 59 (2, Part 2), 1325–1331. https://doi.org/10.1016/j.lwt.2014.03.033.
- Porto, B.C., Cristianini, M., 2014a. Evaluation of cashew tree gum (Anacardium occidentale L.) emulsifying properties. LWT Food Sci. Technol. 59 (2 Part 2), 1325–1331. https://doi.org/10.1016/j.lwt.2014.03.033.
- Rincón, F., Muñoz, J., León de Pinto, G., Álfaro, M.C., Calero, N., 2009. Rheological properties of Cedrela odorata gum exudate aqueous dispersions. Food Hydrocoll. 23 (3), 1031–1037. https://doi.org/10.1016/j.foodhyd.2008.08.006.
- Sakthivel, R., Mallika, J., 2016. A single pot green synthesis of ZnO nanoparticles using aqueous gum exudates of Azadirachta indica and its antifungal activity. Int. J. Res. Eng. Technol. 3 (9), 300–306.
- Samrot, A.V, Angalene, J.L.A., Roshini, S.M., Stefi, S.M., Preethi, R., Raji, P., Madan Kumar, A., Suresh Kumar, S., 2020. Purification, characterization and exploitation of Azadirachta indica gum for the production of drug loaded nanocarrier. Mater. Res. Express 7 (5), 55007. https://doi.org/10.1088/2053-1591/ab8b16.
- Sesták, J. (1984). Thermophysical properties of solids: their measurements and theoretical thermal analysis.
- Simas-Tosin, F.F., Barraza, R.R., Petkowicz, C.L.O., Silveira, J.L.M., Sassaki, G.L., Santos, E.M.R., Gorin, P.A.J., Iacomini, M., 2010. Rheological and structural characteristics of peach tree gum exudate. Food Hydrocoll. 24 (5), 486–493. https://doi.org/10.1016/j.foodhyd.2009.12.010.
- Simas-Tosin, F.F., de Souza, L.M., Wagner, R., Pereira, G.C.Z., Barraza, R.R., Wendel, C. F., Sassaki, G.L., Iacomini, M., Gorin, P.A.J., 2013. Structural characterization of a glucuronoarabinoxylan from pineapple (Ananas comosus (L.) Merrill) gum exudate. Carbohydr. Polym. 94 (1), 704–711. https://doi.org/10.1016/j.carbpol.2012.12.059.
- Singh, A.K., Selvam, R., & Sivakumar, T. (2010). Isolation, characterisation and formulation properties of a new plant gum obtained from Mangifera indica. https:// api.semanticscholar.org/CorpusID:138378548.
- Singh, B., Sharma, V., 2014. Influence of polymer network parameters of tragacanth gum-based pH responsive hydrogels on drug delivery. Carbohydr. Polym. 101, 928–940. https://doi.org/10.1016/j.carbpol.2013.10.022.
- Skreiberg, A., Skreiberg, Ø., Sandquist, J., Sørum, L., 2011. TGA and macro-TGA characterisation of biomass fuels and fuel mixtures. Fuel 90 (6), 2182–2197. https://doi.org/10.1016/j.fuel.2011.02.012.
- Slathia, S., Gupta, T., Chauhan, R.P., 2021. Green synthesis of Ag–ZnO nanocomposite using Azadirachta indica leaf extract exhibiting excellent optical and electrical properties. Phys. B: Condens. Matter 621, 413287. https://doi.org/10.1016/j. physb.2021.413287.
- Takase, M., Zhao, T., Zhang, M., Chen, Y., Liu, H., Yang, L., Wu, X., 2015. An expatiate review of neem, jatropha, rubber and karanja as multipurpose non-edible biodiesel resources and comparison of their fuel, engine and emission properties. Renew. Sustain. Energy Rev. 43, 495–520. https://doi.org/10.1016/j.rser.2014.11.049.
- Vinod, V.T.P., Sashidhar, R.B., Suresh, K.I., Rama Rao, B., Vijaya Saradhi, U.V.R., Prabhakar Rao, T., 2008. Morphological, physico-chemical and structural characterization of gum kondagogu (Cochlospermum gossypium): a tree gum from India. Food Hydrocoll. 22 (5), 899–915. https://doi.org/10.1016/j. foodhyd.2007.05.006.
- Wesley William Wendlandt. (1974). Thermal methods of analysis (Second). John Wiley and Sons, New York, cop.
- White, J.L., 1971. Interpretation of infrared spectra of soil minerals. Soil Sci. 112 (1), 22–31. https://doi.org/10.1097/00010694-197107000-00005.
- Xu, F., Yu, J., Tesso, T., Dowell, F., Wang, D., 2013. Qualitative and quantitative analysis of lignocellulosic biomass using infrared techniques: a mini-review. Appl. Energy 104, 801–809. https://doi.org/10.1016/j.apenergy.2012.12.019.
- Zhou, H., Long, Y., Meng, A., Li, Q., Zhang, Y., 2013. The pyrolysis simulation of five biomass species by hemi-cellulose, cellulose and lignin based on thermogravimetric curves. Thermochim. Acta 566, 36–43. https://doi.org/10.1016/j.tca.2013.04.040.